NeuroImage 220 (2020) 117071

Contents lists available at ScienceDirect

NeuroImage

journal homepage: www.elsevier.com/locate/neuroimage

Should I stay or should I go? How local-global implicit temporal expectancy shapes proactive motor control: An hdEEG study

G.M. Duma [a,c,*], U. Granziol [a], G. Mento [a,b]

[a] Department of General Psychology, University of Padova, Italy
[b] Padua Neuroscience Center (PNC), University of Padova, Italy
[c] Scientific Institute, IRCCS "E. Medea", Association "La Nostra Famiglia", Conegliano, TV, Italy

ARTICLE INFO

Keywords:
Dynamic temporal prediction task
Proactive response adjustment
Anticipatory ERP activity
Probabilistic context

ABSTRACT

In this study, we investigated the effect of global temporal prediction on the brain capability to implicitly adjust proactive motor control. We used the Dynamic Temporal Prediction (DTP), in which local and global predictions of an imperative stimulus were manipulated by using different stimulus-onset asynchronies (SOAs), presented with several distribution probabilities. At a behavioural level, the results show a performance adjustment (reaction time decrease) depending on the implicit use of global prediction. At a neurophysiological level, three separate computational steps underlying motor control were investigated. First, the expectancy implementation was associated with global probability-dependent contingent negative variation (CNV) modulation supported by the recruitment of a frontoparietal network involving the anterior cingulate, the left intraparietal sulcus, the occipital, and the premotor areas. Second, the response implementation was modulated by the global prediction fostering stimulus processing (P3 increase) at the motor response level, as suggested by both oscillatory (beta desynchronization), as well as source analysis (frontal cortical network). Third, the expectancy violation lead to a negativity increase (omission-detection potential) time locked to the global rule violation and additionally, to delta and theta power increase interpreted as inhibitory control and rule violation detection, respectively. The expectancy violation further engaged a left lateralized network including the temporal parietal junction (TPJ) and the motor cortex, suggesting involvement of attentional reorienting and a motor adjustment. Finally, these findings provide new insights on the neurocognitive mechanisms underlying proactive motor control, suggesting an overlapping between implicit and explicit processes.

1. Introduction

The ability to control our motor behaviour by preactivating (proactive control) or stopping (reactive inhibition) a response to task-relevant stimuli is shaped by both top-down, explicit instruction and bottom-up, implicit factors that may be unbeknownst to participants (Braem and Egner, 2018). Among these, the possibility to exploit either *local* or *global* temporal regularities to generate and update a prediction about the temporal onset of an imperative stimulus is crucial (Nobre and Van Ede, 2018; Bekinschtein et al., 2009; Chennu et al., 2013; Marti et al., 2014). Indeed, local and global statistical rules represent hierarchically-nested orders of information that can be extracted from sequential patterns and used to build-up a predictive internal model of world's regularities and, consequently, bias attention and action. In this study we investigated how distinct neurocomputational mechanisms underlying motor control are affected by the implicit use of global temporal prediction.

Specifically, in a sequence of sensory events, the local prediction refers to the stimulus expectancy bias induced by the narrow transitional probabilities, which do not need a long-term, 'historical' statistical knowledge. By contrast, the *global* prediction refers to the ability to extract higher-level rules besides local transitions. In the case of motor preparation, the local prediction can be identified as the effect of the stimulus hazard rate on reaction times (RTs). In fact, the subjective probability of a stimulus onset will increase over time given that it has not occurred yet (Karlin, 1958; Los, 2010; Luce, 1986; Niemi and Näätänen, 1981; Nobre et al., 2007; Woodrow, 1914). For instance, in the case of three discrete foreperiod (FP) intervals (e.g., 0.5, 1 or 1.5 s) participants will be significantly fastest at detecting targets occurring at the shortest FP (for a review, see Los, 2010). By contrast, global prediction refers to the history-driven probability of an event occurrence in the long period (Baumeister and Joubert, 1969; Los

* Corresponding author. Department of General Psychology, University of Padova, Via Venezia 8, 35129, Padova, Italy.
E-mail addresses: gianmarco.duma@unipd.it (G.M. Duma), umberto.granziol@unipd.it (U. Granziol), giovanni.mento@unipd.it (G. Mento).

https://doi.org/10.1016/j.neuroimage.2020.117071
Received 26 March 2020; Received in revised form 12 June 2020; Accepted 17 June 2020
Available online 20 June 2020

et al., 2017; Trillenberg et al., 2000). Indeed, participants become faster to detect shortly-expected targets when these are globally more probable to occur. By contrast, a low global probability to receive a short preparatory interval implies a slowing down of RTs to stimuli presented at short FPs (Los et al., 2017; Trillenberg et al., 2000). In summary, the way participants will prepare to respond to an upcoming event will depend not only on how long they are waiting it (hazards rate or local prediction) but also on when this event is overall more likely to occur on the basis of past experience (global prediction). The first one operates *within-trial* while the second one *across-trials* and are supposed to exert independent but interactive effects on subjective temporal expectancy and motor control.

1.1. Temporal prediction turns into specific expectancy-related brain activity

A functional implication of the ability to make use of temporal prediction consists in the possibility to translate this knowledge into stimulus anticipatory brain activity (Cui et al., 2009; Mento, 2013; Miniussi et al., 1999), a computational stage defined as *expectancy implementation* (Mento and Vallesi, 2016; Cotti et al., 2011). One of the most reliable neural marker of expectancy implementation is the Contingent Negative Variation or CNV, a sustained event-related potential (ERP) arising between two contingently associated sensory events and reflecting anticipatory processes (Walter et al. 1964; Mento et al., 2013; Mento, 2017). The CNV is locally enhanced following explicit predictive cues (Miniussi et al., 1999; Mento et al., 2015; Correa et al., 2006; Capizzi et al., 2013) but also implicit predictive information (Coull and Nobre, 2008) such as temporally regular vs. irregular target presentation (Breska and Deouell, 2014; Praamstra et al., 2006), sequential effects (Los and Heslenfeld, 2005; Mento, 2017; Capizzi et al., 2013) or simple associative learning (Mento et al., 2013; Mento and Valenza, 2016). While the neural generators of this component are not entirely known, there is converging evidence that a distributed fronto-parietal cortical network mainly including the premotor, the supplementary motor and the parietal areas is involved in its generation (Mento et al., 2013, 2015; Mento, 2017; Macar and Vidal, 2004).

In line with behavioural evidence, the pre-allocation of neural activity translates into the convey of attentional and motor resources to task-relevant stimuli, a mechanism that can be defined as *response implementation*. In the context of motor preparation tasks, this is revealed by the larger post-stimulus late ERP amplitude (i.e., the P3 response) following predicted than unpredicted stimuli (Capizzi et al., 2013; Doherty et al., 2005; Correa and Nobre, 2008; Mento, 2017; Nobre, 2001; Zanto et al., 2011).

Finally, besides translating prediction into anticipatory activity, in order to flexibly adjust the behavioral outcome, the brain must also be able to online update its internal predictive models according to the incoming environmental stimuli and requests (Friston, 2010). This implies that when the system experiences an error prediction, such as in the case of *expectancy violation*, the internal model needs to be updated (Friston, 2010; Clark, 2013; Wacongne et al., 2012; Visalli et al., 2019; Zandbelt et al., 2013). The possibility to gain advantage from errors allows indeed to re-tune perceptual and motor processes toward an optimal re-preparation. This is what happens, for instance, when a response is prepared shortly but must be stopped since the stimulus actually arrives late. While expectancy implementation, response implementation and expectancy violation are crucial mechanisms for regulating motor control, only few studies have tried to address the question whether these distinct computational stages are differently modulated by local *vs.* global prediction.

Noteworthy, while the effect of local prediction on motor control has been well elucidated (Miniussi et al., 1999; Coull et al., 2011; Mento et al., 2015; Mento, 2017; Vallesi, 2010), as far as we know, only few studies investigated the effect of global prediction on motor control. Among these, Trillenberg et al. (2000) reported a CNV amplitude modulation related to the FP probability distribution. Though, this study examined the effect of global probability neither on the response implementation nor on the violation expectancy. On the other side, in a recent study Visalli et al. (2019) adopted a bayesian computational approach and a neuroimaging method (fMRI) to map the neural correlates of the updating of temporal expectations in the human brain. Notably, in both the studies mentioned above, the authors provided participants with explicit instructions about the change in the global FP properties. Hence, the question whether implicit proactive motor control draws on similar neural mechanisms as those described for explicit control is still to be addressed.

To this purpose we recorded and analyzed the high-density electroencephalographic (hdEEG) activity from healthy participants undergoing the Dynamic Temporal Prediction task (DTP; Mento and Granziol, 2020; Mento et al., 2020). The DTP is a task consisting in a changed version of the variable FP task (Niemi and Naatanen, 1981; Los, 2010; Vallesi, 2010; Woodraw, 1914) purposely modified to introduce different hierarchies of stimulus predictability. In particular, we manipulated block-wise the probability distribution of three discrete FP intervals in order to generate a global expectation bias toward either the short or the long FP. To shed light on the neural bases of implicit proactive motor control we provided a multiple-domain brain investigation. In particular, we analyzed the ERP activity to depict the effects of global prediction on the temporal locus of expectancy implementation, expectancy violation and response implementation as three temporally distinct computational stages underlying proactive motor control. We also explored the oscillatory patterns to shed light on the functional dynamics in terms of neural synchronization/desynchronization induced by global task properties. Finally, we reconstructed the spatial geography of the same effects at the source-level to provide a whole picture of the phenomena and compare our findings with previous neuroimaging literature.

To investigate how global prediction affects expectancy implementation, we targeted the Contingent Negative Variation (CNV) in relation to the global probabilistic context. In line to the results reported by Trillenberg et al. (2000), we expected to find a CNV increase related to the global prediction, so that, for the same interval, a block-wise higher percentage of FP should lead to a large CNV amplitude. To test the effect of prediction on response implementation we targeted stimulus-locked neural activity. As previously shown for explicit temporal prediction (Capizzi et al., 2013; Doherty et al., 2005; Mento, 2017), we expected to observe a global-dependent modulation of the late ERPs (P3 component) reflecting massive recruitment of motor resources. Finally, the expectancy violation was investigated by targeting the omission-evoked potential elicited by the missed presentation of the target at the time when it was expected based on global prediction. In this case the we hypothesized the onset of the omission potential synchronized with the rule violation (i.e. the stimulus was supposed to appear after 500 ms, but the onset was delayed at 1500). To further unravel the neural mechanisms underlying the effect of global prediction on proactive motor control we also investigated the event-related oscillatory activity. According to previous literature we hypothesized the involvement of the delta, theta and beta frequency bands. Specifically, we expected the global prediction to instantiate a beta power desynchronization in both the prestimulus (expectancy implementation) and postimulus (response implementation) windows (Jasper and Penfield, 1949; Tzagarakis et al., 2010; Pfurtscheller and Berghold, 1989; Sanes and Donoghue, 1993; Murthy and Fetz, 1996; Pfurtscheller and Neuper, 1997; Formaggio et al., 2008). Furthermore, we expected a modulation of delta and theta bands, especially considering their relation with inhibitory control (Prada et al., 2014) and expectancy violation (Cavanagh and Frank, 2014), respectively. More specifically, we expected to observe a delta and theta rule violation-dependent power increase, as previously demonstrated for endogenously-driven motor control. Finally, we performed the source reconstruction of all significant ERP effects to further depict the underlying neural generators in the spatial domain.

2. Method

2.1. Participants

The sample size was a priori computed with G*Power3 (Faul et al., 2007). Starting from the effect size reported in Mento and Granziol (2020) and Mento et al. (2020) we defined an effect size of d = 0.45. Sample size was computed using a two tails t-tests as Test family, α = 0.05; power (1-β) = 0.90, resulting in a total sample of 44 participants. Data were collected from 50 healthy adult participants. Two participants were excluded due to equipment failure. The final sample included 48 participants (mean age = 22.96 years, [SD = 1.14], range 20–27, 8 males). All participants reported normal or corrected-to-normal vision and had no history of neurological and/or psychiatric disorders. All participants gave their informed consent before the experiment. All experimental procedures were approved by the Ethics Committee of the School of Psychology at the University of Padua (protocol n° 2536) and were conducted according to the principles expressed in the Declaration of Helsinki.

2.2. Experimental procedure

Stimuli were presented on a 17-inch monitor at a resolution of 1280 × 1024 pixels. Participants were seated comfortably in a chair at a viewing distance of around 60 cm from the monitor. All participants performed a warned simple reaction time (RT) task adapted from an experimental paradigm previously employed from our lab to investigate voluntary and automatic temporal attention effects in adults and school-aged children (Mento and Tarantino, 2015). This task, defined as Dynamic Temporal Prediction (DTP) (Mento and Granziol, 2020; Mento et al., 2020) was originally conceived to investigate children's behavioral performance in relation to either local or global probabilistic rules as two distinct sources of temporal predictability. We used here a modified version adapted for ERP investigation.

2.3. Trial structure

Each trial began with the display of a warning visual stimulus (S1), followed by the presentation of an imperative visual stimulus (S2) that stayed on the screen for a maximum of 3000 ms. S1 consisted of a picture of a black camera lens (see Fig. 1) surrounded by a circle (total size of the stimulus: 840 × 840 pixels, 144 dpi, 10.62° × 10.54° of visual angle). S2 consisted of a picture of a cartoon character, which was displayed centrally within the camera lens. The inter-trial-interval was randomly manipulated between 600 and 1500 ms. The task consisted of speeded target detection. Participants were required to press a button of the response box with the index finger of the dominant hand as quickly as possible at S2 occurrence.

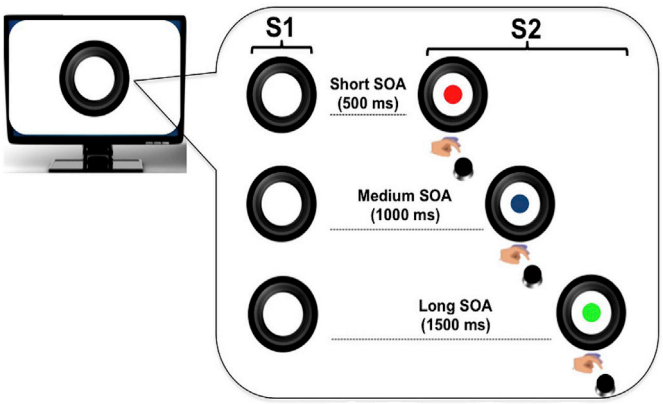

Fig. 1. Trial structure. The circle (S1) warned participants on the presentation of the imperative S2 stimulus (a cartoon character; here represented with colored disks for illustrative purposes due to copyright restriction). Participants had to make speeded reaction times at S2 onset by pressing a button on the keyboard. The effect of local prediction was assessed by manipulating S1–S2 stimulus onset asynchrony (SOA) within each experimental block.

2.4. Local predictive context

To investigate the effect of the local predictive context on behavioral performance, the S1–S2 stimulus-onset-asynchrony (SOA) was varied trial by trial within each experimental block so that three possible fixed FP intervals were created (Fig. 1). These included a short (500 ms), a medium (1000 ms), or a long (1500 ms) FP, resulting in three discrete levels of hazard rate. (Karlin, 1958; Los, 2010; Luce, 1986; Niemi and Näätänen, 1981; Woodrow, 1914).

2.5. Global predictive context

As illustrated in Fig. 2, to assess the effect of the global changes in the predictive context, different probability distributions per each SOA interval were introduced and manipulated block-wise, as described below.

2.5.1. Uniform (U) block

In this block, a rectangular distribution of the three SOAs was used (33,3%, for each SOA) so that the probability of each SOA in the block was equally distributed. This type of distribution is the most classic probabilistic distribution employed in both adult (Los, 2010; Mento, 2017; Mento et al., 2015; Vallesi, 2010) and developmental (Johnson et al., 2015; Mento and Tarantino, 2015; Mento and Vallesi, 2016; Vallesi and Shallice, 2007) SOA literature.

The use of an a priori uniform distribution has long been described to translate into a biased a posteriori temporal preparation. Indeed, as time goes by, the conditional probability of S2 onset increases exponentially in virtue of the fact that it has not occurred yet (Los, 2010; Los et al., 2017; Luce, 1986). As a consequence, motor preparedness will be lowest at the shortest SOA and highest at the longest SOA.

2.5.2. Short-biased (SB) block

In this case, an a priori distribution biased toward the short SOA was delivered. In particular, the relative percentage was 50%, 33,33%, and 16,67% for the short, medium, and long SOA, respectively.

2.5.3. Long-biased (LB) block

In this block, the relative percentage was 16,7%, 33,3%, and 50% for the short, medium, and long SOA, respectively. This kind of distribution, also known in the literature as aging distribution (Los et al., 2017; Trillenberg et al., 2000), is purposely intended to exacerbate the hazard-based increment of temporal expectancy as a function of SOA length.

2.6. Experimental design

The experimental manipulations yielded a factorial design in which either the SOA (short *vs.* medium *vs.* long) and the block type (SB *vs.* U *vs.* LB) factors were orthogonally contrasted to investigate the effect of local and global predictive context, respectively (Fig. 2).

Each single block included 60 trials and was delivered three times, for a total of nine experimental blocks and 540 trials. Specifically, the number of trial were 90, 60 and 30 for SB-S, SB-M and SB-L conditions, respectively; 60 trials for each SOA in the U block and 30, 60 and 90 trials for LB-S, LB-M and LB-L conditions, respectively. All blocks were matched for sensorimotor requirements, as the visual stimuli and the required response were always the same across the experiment. The only differences were related to the changes in the predictive context experienced through the task. The total length of the experiment was about 25 min. It is important to note that participants were unbeknownst of both local and global manipulations since no explicit information were given about this.

		LOCAL		
		Short (S) (500 ms)	Medium (M) (1000 ms)	Long (L) (1500 ms)
GLOBAL	Short-biased (SB)	50% (SB-S)	33,3% (SB-M)	16,7% (SB-L)
	Uniform (U)	33,3% (U-S)	33,3% (U-M)	33,3% (U-L)
	Long-biased (LB)	16,7% (LB-S)	33,3% (LB-M)	50% (LB-L)

Fig. 2. Experimental Design. The effect of global prediction was assessed by manipulating the between-block, a priori percentage of each SOA to create three probabilistic distributions in which the SOAs were equally distributed (uniform) or skewed toward the short (short-biased) or long (long-biased) SOA.

Furthermore, no pauses were introduced between blocks. Instead, a blank slide was inserted at the middle of each block to allow participant to rest. In this way we avoided participants to become aware about global changes occurring at any block switch. The block-type order was randomly sorted between subjects. This ensured that spurious effects due to introducing either local or global predictive contexts induced by a fixed SOA or block sequence did not bias the performance. To ensure that the experimental manipulation was effective in inducing implicit prediction, after completing the task we asked all participants if they realized that the task could change in speed, becoming faster or slower over time. Before starting the experimental session, participants were presented with a block of 20 training trials for each condition to ensure they understood task instructions. During training, all participants received a feedback at every trial according to their performance. Specifically, a neutral yellow smile was displayed in cases in which either anticipatory (before target onset) or premature (<150 ms before target onset) responses were provided. A yellow smile was displayed if the RT was between 1000 and 1500 ms from target onset. Finally, a green smile was displayed if the RT was between 150 and 1000 ms. E-prime 2 software (Psychology Software Tools, Pittsburgh, USA) was used to create and administer the stimuli. Behavioral data are available on Figshare public repository (10.6084/m9.figshare.12246218).

2.7. Behavioral analysis

We used mean accuracy and mean RTs as response variables on which testing our hypotheses. In particular, accuracy refers to the mean percentage of not anticipated responses across all experimental conditions (i.e., between 150 ms and 1500 ms from target onset). To calculate response speed, we considered only RTs measured in correct trials, i.e., without premature responses. We analyzed the effects on response accuracy and speed by setting a 3 × 3 within subject experimental design, that we tested through generalized linear mixed-effect models (GLMMs). In particular, we defined two separate GLMMs for response speed and accuracy, respectively. Both SOA (i.e., Short *vs.* Medium *vs.* Long) and block (i.e., SB *vs.* U *vs.* LB) were considered within subject fixed factors. We set random intercept models, with participants as the clustering variable. We adopted the procedure suggested by Westfall, Kenny, and Judd (2014) to calculate Cohen's d for each comparison used the R statistical software (R Core Team, 2018) to run statistical analyses, using the following packages: lme4 (Bates et al., 2015) to test the GLMMs, emmeans (Lenth, 2018) to test multiple comparisons and car (Fox and Weisberg, 2011) to estimate p-value, which were adjusted with a false discovery rate correction (Benjamini and Hochberg, 1995). Behavioral analysis code is available on Figshare (10.6084/m9.figshare.12249302).

2.8. EEG recordings

We used a Geodesic high-density EEG System (EGI® GES-300) with a pre-cabled 128-channel HydroCel Geodesic Sensor Net (HCGSN-128) and electrical reference to the vertex. EEG data were recorded during the entire experiment. The sampling rate was 500 Hz. The impedance was kept below 60 kW for each sensor. In order to reduce signal contamination, participants were instructed to limit eye blinks and eye movements as much as possible during task trials. EEG data are available on Figshare public repository (10.6084/m9.figshare.12246218).

2.8.1. EEG preprocessing

Signal preprocessing was performed through EEGLAB 14.1.2b (Delorme and Makeig, 2004). The continuous EEG signal was first downsampled at 250 Hz and then bandpass-filtered (0.1–45 Hz) using a Hamming windowed sinc finite impulse response filter (filter order = 8250). The signal was successively epoched between −500 and 1996 ms from S1 onset. Epochs related to trials containing premature responses were rejected. Epoched data were subjected to an automated bad-channel and artifact detection algorithm by using the TBT plugin (Ben-Shachar, 2020) implemented in EEGLAB. This algorithm identified the channels that exceeded a differential average amplitude of 250 μV and marked those channels for rejection. Channels that were marked as bad on more than 30% of all epochs were excluded. Epochs having more than 10 bad channels were also excluded. Successively, we automatically detected possible flat channels with the Trimoutlier EEGLAB plug in, with the lower bound of 1 μV. Data cleaning was performed by means of an independent component analysis (Stone, 2002), using the Infomax algorithm (Bell and Sejnowski, 1995) implemented in EEGLAB. The resulting independent components were visually inspected in topography and time-series, and those related to eye blinks, eye movements and muscle artifacts were discarded. The remaining components were then projected back to the electrode space to obtain cleaner EEG epochs. Finally, bad channels were reconstructed with the spherical spline interpolation method (Ferree, 2006; Perrin et al., 1989). The data were then re-referenced to the average of all electrodes, and baseline correction was applied by subtracting the mean signal amplitude in the pre-stimulus interval. Epoched data were imported in Brainstorm (Tadel et al., 2011) to generate the individual average for each electrode site and experimental condition. We applied a weighted average in order to control for the unbalanced number of epochs per condition (Kotowski et al., 2019; Lęski, 2002). The mean number of epochs and standard deviation (SD) in brackets for each condition are listed in Table 1.

2.8.2. Oscillatory EEG analysis

The oscillatory activity of each trial was calculated using Morlet wavelet analysis (central frequency = 1 Hz; time resolution (FWHM) = 3

Table 1
Mean number of trials and standard deviation between brackets of each experimental condition.

SB-S = 89,29 (3,30)	SB-M = 57, 35 (2,55)	SB-L = 28,91 (1,42)
U–S = 56, 26 (3,33)	U-M = 57,58 (2,71)	U-L = 57,14 (2,93)
LB-S = 28,66 (1,68)	LB-M = 56,25 (3,10)	LB-L = 85,89 (3,96)

s) using the Brainstorm software. The time-frequency (TF) activity was studied from 1 to 45 Hz, diving the frequency range in 60 bins with a logarithmic frequency definition. Data were then averaged obtaining a TF map for each subject and each experimental condition. Successively, event related synchronization/desynchronization percentage (ERSD) was calculated, according to Pfurtscheller and Lopes (1999), by using the following formula: ERS/ERD = $(E\text{-}\mu)/\mu \times 100$ where E indicates the power density during the event condition and μ indicates the mean of the power density during the baseline. Finally, we grouped TF maps in frequency bands by averaging the power spectrum density as it follows: Delta (2–4 Hz); Theta (5–7 Hz), Alpha (8–12 Hz); Beta1 (13–21 Hz), Beta2 (21–30 Hz), Gamma (30–45 Hz).

2.8.3. Cortical source modelling

Baseline-corrected epochs were imported in Brainstorm (Tadel et al., 2011) to model their cortical generators. We used the ICBM152 anatomical template to approximate the individual anatomy of each participant (Evans et al., 2012). Co-registration of EEG electrodes position was performed via Brainstorm, by projecting the digitized EEG sensor positions GSN Hydrocel 128 E1 available in Brainstorm on the head surface. We then derived an EEG forward model using the three-layer boundary element method (BEM) from OpenMEEG implemented as a Brainstorm routine (Kybic et al., 2005; Gramfort et al., 2011). The source space was constrained to the cortex and modeled as a grid of 15.002 orthogonal current dipole triplets. We used sLORETA as a source model, with Brainstorm's default parameter settings. The empirical noise covariance model was obtained from the average of ERP baseline signals. The sources were projected to the standard anatomical template (MNI) and their activity was transformed in Z scores relative to the baseline. Finally, a spatial smooth with a FWHM of 3 mm, was applied to each source.

2.9. EEG statistical analysis

We applied a whole-scalp analysis approach at all electrode sites using a paired *t*-test (α = .05) permutation approach to control the family-wise error rate (Groppe et al., 2011). A similar technique was employed in previous ERP studies (Duma et al., 2019; Mento et al., 2018; Mento, 2017; Strauss et al., 2015; Capizzi et al., 2016). To control for the 1-type error we performed 2000 Monte-Carlo permutations and applied cluster-based

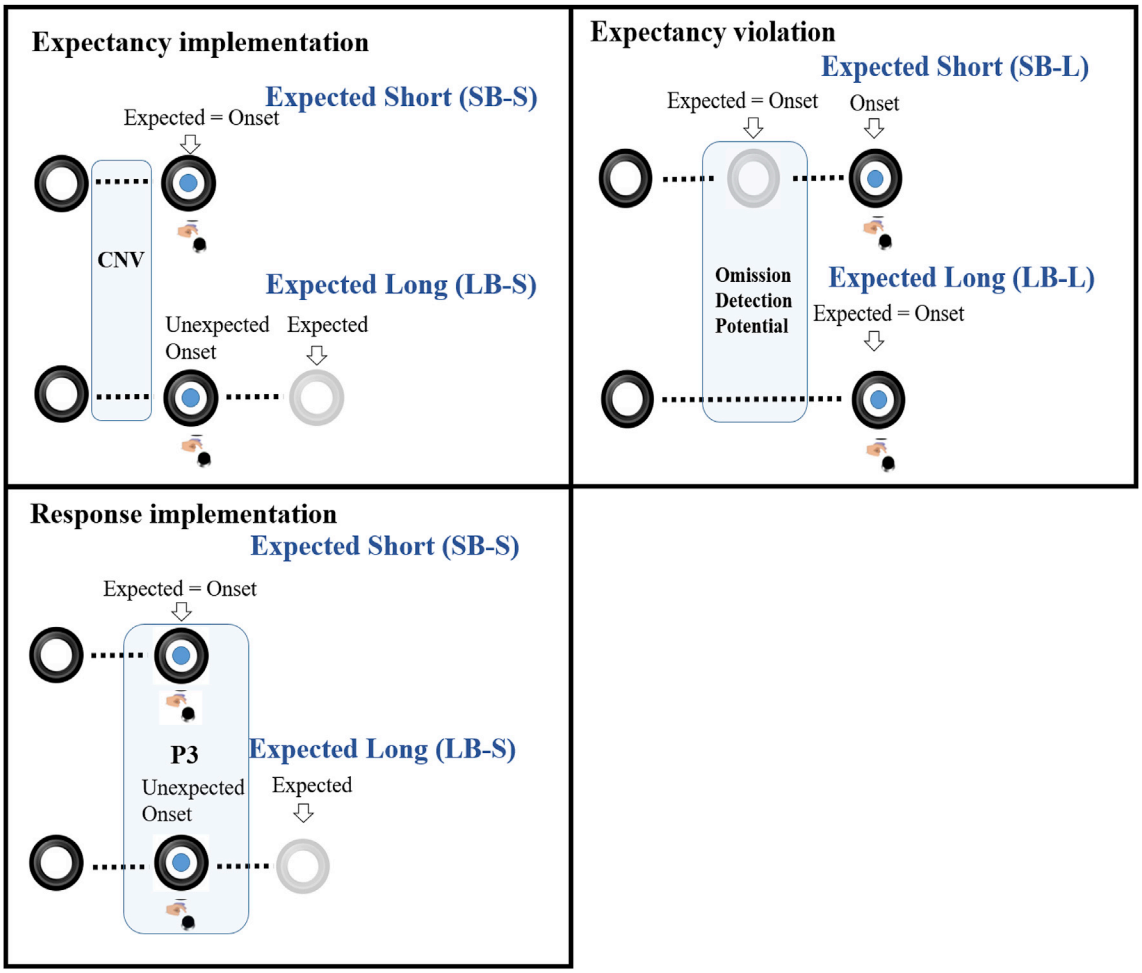

Fig. 3. Temporal windows of interest for the statistical analyses. A) Expectancy implementation was investigated by comparing the CNV amplitude in the last 100 ms of the preparatory activity. B) Expectancy violation was tested by contrasting the condition where the global probabilistic rule was violated SB-L in which the stimulus occurs before the expected onset) against the LB-L condition, in which the global probability was respected. We expected to find an ODP wave for the SB-L condition. C) Response implementation was examined in the P3 time window, comparing the condition with maximum expectancy (SB–S) to the one with the lowest expectation (LB-S).

correction over all 128 electrode locations using the Fieldtrip functions (Oostenveld et al., 2011), accessible via Brainstorm (Tadel et al., 2011). The ERP effect size was estimated by computing Cohen's d of the effect averaged over all the electrodes included in the significant clusters for each comparison (Buiatti et al., 2019). Our experimental manipulation allowed us to test specific hypotheses about the effect of the global predictive context on distinct cognitive mechanisms underlying proactive motor control. These encompassed expectancy implementation, expectancy violation and response implementation (Fig. 3). The EEG analysis pipeline, with all the computational steps and the functions used from EEGLAB (Delorme and Makeig, 2004) and Brainstorm (Tadel et al., 2011), is available on Figshare (10.6084/m9.figshare.12249302).

2.9.1. Expectancy implementation

To investigate the functional locus of expectancy implementation, the Contingent Negative Variation (CNV; Walter et al., 1964; Mento, 2013) was targeted as a neural signature of response preparation and measured in the last 100 ms of the preparatory activity, from S1 onset (Mento, 2017). In line with previous findings (Trillenberg et al., 2000), we speculated that the CNV was affected by the global predictive context, resulting in larger amplitude for the SB-S as compared to the LB-S.

2.9.2. Response implementation

Finally, in order to investigate response implementation, we examined the post target onset activity comparing SB-S and LB-S conditions. Specifically, we expected a modulation in the amplitude of the P3 potential. Therefore, we focused on the mean activity between 250 and 400 ms from S2 onset, where the P3 is usually expressed.

2.9.3. Expectancy violation

As shown in Fig. 3b, in our task the expectancy violation occurred in the SB-L condition, since in this case the participants were implicitly biased to expect the imperative stimulus at the short SOA but this was actually delivered at a longer interval. A violation of the learnt global probabilistic rule should yield to a more difficult inhibition of the motor response since this had been proactively maximally prepared. At the behavioural level, we expected to find the lowest accuracy (i.e., more premature responses) in the SB-L condition. The neurofunctional correlates (both ERP and oscillatory activity) of the expectancy violation were investigated between 100 and 200 ms from the missed S2 onset (i.e., 600–700 ms from S1 onset). In particular, we expected to find a global omission-detection potential (ODP) similar to the one we reported for local expectancy violation in our previous study using a similar task (Mento and Vallesi, 2016). In order to partial out any potential diverging pre-S1 baseline slopes deriving from different SB-LB inter-trial preparatory effects, we applied a baseline correction over the entire pre-target time window (0–1500 ms) of the long SOA.

The permutation statistic with cluster correction was also applied in the statistical analyses of oscillatory activity in the same temporal windows of the ERP analysis. Finally, concerning the source statistic, a permutation paired *t*-test was run over the mean amplitude of the Z-scored maps, in the same window of interest of the ERP and oscillatory analyses.

3. Results

3.1. Behavioral results - accuracy

As expected, the mean accuracy was affected by the local predictive context. This was revealed by the effect of the SOA ($\chi^2_{(2)} = 54.99$; $p < .001$). Specifically, participants were more accurate in trials with short than medium ($t_{(376)} = 2.56$; $p = .03$; $d = 0.27$) or long SOA ($t_{(376)} = 7.31$; $p < .001$; $d = 0.79$) as well as in medium than long SOA trials ($t_{(376)} = 4.74$; $p < .001$; $d = 0.51$) (degrees of freedom are calculated accordingly to the kenward-roger approximation; Kenward and Roger, 1997). The mean accuracy was affected by the global predictive context, as suggested by the significant effect of the Block ($\chi^2_{(2)} = 15.34$; $p < .001$). The participants showed overall lower accuracy in the SB than in the U ($t_{(376)} = -3.44$; $p < .01$; $d = 0.37$) or the LB blocks ($t_{(376)} = -3.39$; $p < .001$; $d = 0.36$). On the contrary, the accuracy was not statistically different between the U and the LB blocks ($t_{(376)} = -0.1$; $p = .99$; $d = 0.01$). We also found a statistically significant SOA × Block interaction ($\chi2_{(4)} = 15.34$; $p < .001$). As shown in Fig. 4, this was explained by lower accuracy in the SB as compared to the LB ($t_{(376)} = -5.05$; $p < .001$; $d = 0.95$) or U blocks ($t_{(376)} = -5.11$; $p < .001$; $d = 0.96$), but only for long SOA trials. All the other differences did not reach statistical significance.

3.1.1. Reaction times

Also for RTs we observed a statistically significant effect of SOA on RTs ($\chi^2_{(2)} = 870.4$; $p < .001$), so that participants were faster in trials with long than medium ($z = -6.15$; $p < .001$; $d = 0.51$) or short ($z = -28.93$; $p < .001$; $d = 2.63$) SOA (with model fitting asymptotic distribution, the emmeans package computes z statistics to calculate multiple comparisons). Participants were also faster in medium than short SOA trials ($z = -22.94$; $p < .001$; $d = 2.12$). We observed a statistically significant effect of Block on the RTs ($\chi^2_{(2)} = 63.73$; $p < .001$), since participants were overall faster in SB rather than U ($t_{(376)} = -3.33$; $p < .01$; $d = 0.29$) and LB trials ($t_{(376)} = -8.69$; $p < .001$; $d = 0.77$). Furthermore, participants were overall faster in trials administered within the U than the LB blocks ($z = -5{,}37$; $p < .001$; $d = 0.48$). The SOA × Block interaction ($\chi2_{(4)} = 30.09$; $p < .001$) further confirmed that the global effect affected differently the three SOA intervals. As displayed in Fig. 4b, the participants were faster in the SB as compared to the U ($z = -4.55$; $p < .001$; $d = 0.77$) and the LB ($z = -8.32$; $p < .001$; $d = 1.43$) blocks, as well as in the U as compared to the LB ($z = -3.76$; $p < .001$; $d = 0.66$) blocks. Remarkably, these block-related differences were maximally observed for the short SOA. A similar, but minor effect was also observed for the medium SOA trials, since in this case participants were slower in the LB as compared to the SB ($z = 4.12$, $p < .001$, $d = 0.6$) and uniform ($z = 3.25$; $p < .001$; $d = 0.47$) blocks. No statistically significant block-related differences emerged for the long SOA trials. Importantly, despite the participants' performance was significantly affected by the block-type, none of them reported having noticed this changes, thus confirming that the global prediction had an implicit impact on behaviour.

3.2. EEG results

3.2.1. Expectancy implementation

The permutation analyses in the anticipatory time window in which the expectancy implementation was investigated revealed a negative cluster of centro-parietal electrodes ($p = .04$; cluster size = −43; cluster statistic = 38; $d = -0.32$), which exhibited a negativity increase of the CNV amplitude for the SB-S condition as compared to the LB-S one (see Fig. 5A; Supplementary Fig. 1). No significant results in the frequency domain were found in the same time window of ERP and source analyses. The statistical analyses of the source maps reconstructed over the CNV significant time window showed a larger recruitment of cortical activity in the SB-S compared to the LB-S ($p < .01$). This consisted of a distributed network including the left intraparietal sulcus (IPS), the bilateral supplementary motor area (SMA), the middle and caudal cingulate cortex and the bilateral activation of the cuneus (see Fig. 5B).

3.2.2. Response implementation

The statistical analysis highlighted a significant modulation between 250 and 400 ms showing a mean amplitude increase of the P3 potential expressed over centro-parietal electrodes for the stimuli occurring in the maximally expected temporal interval (SB–S) compared to those presented in the less probable (LB-S) (positive cluster: $p = .010$; cluster size = 70, cluster statistic = 50; negative cluster: $p = .013$; cluster size = 68, cluster statistic = 50; $d = 0.34$) (see Fig. 6A; Supplementary Fig. 1).

The statistical analysis over the TF maps revealed a desynchronization increase in the beta band over frontal electrodes ($p = .008$; cluster size = −182; cluster statistic = 144) with a preferential left lateralization

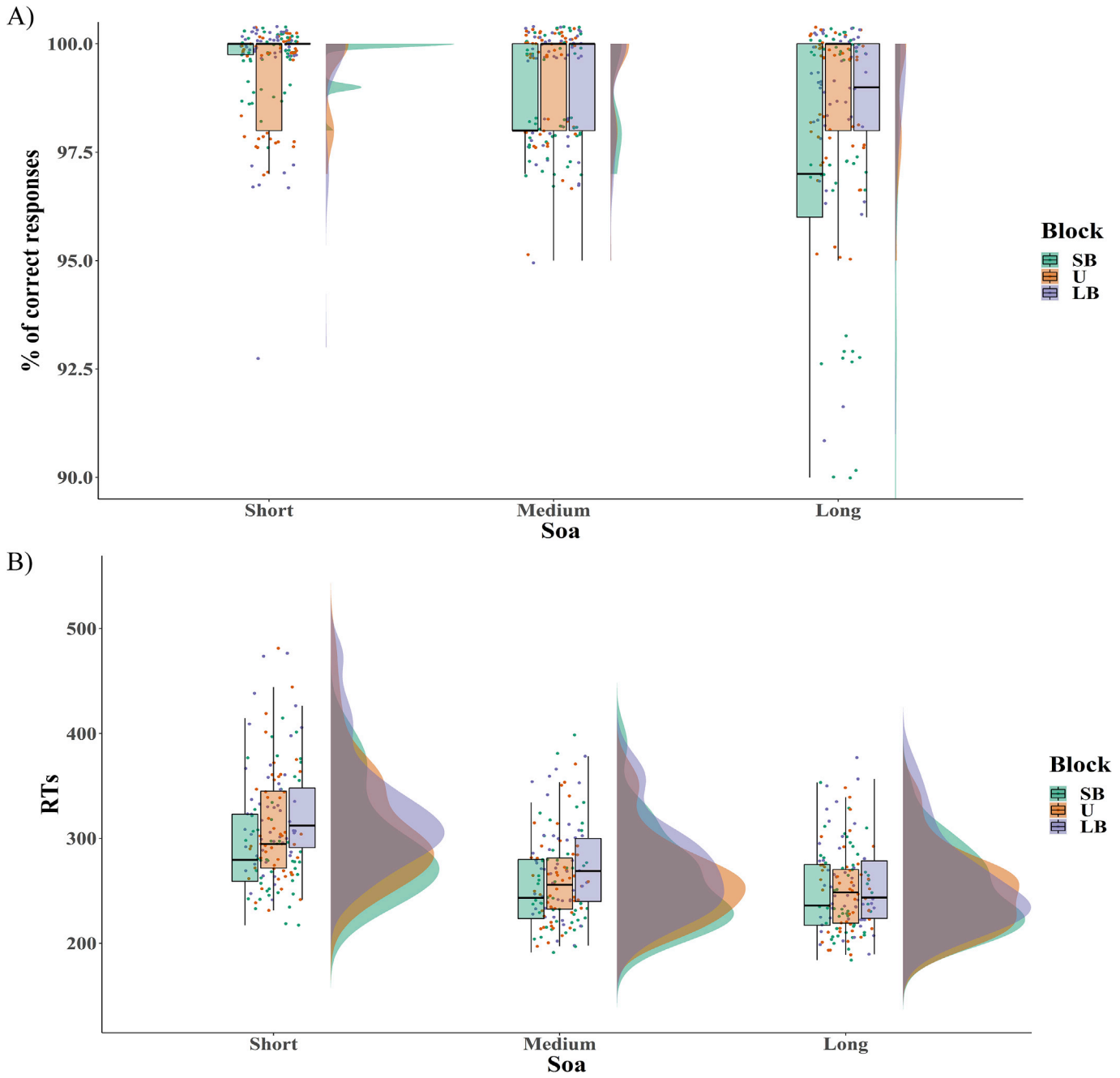

Fig. 4. The figure shows the raincloudes and box plot of the single-subject data for mean accuracy (panel A) and reaction times (panel B) per block-type (SB, U and LB) and SOA (short, medium and long).

(see Fig. 6B). Furthermore, a significant theta desynchronization increase has been identified in the SB-S condition compared to the LB-S over centralized frontal electrodes (p = .008; cluster size = −182; cluster statistic = 144) (see Fig. 6C).

Finally, the source statistic revealed an engagement of a clear-cut network spreading over the bilateral motor and premotor areas as well as over the superior and the middle frontal gyrus (p < .01). Additionally, significant activations have been identified in the cingulate cortex (see Fig. 6D).

3.2.3. *Expectancy violation*

We found a transient, significant negative increase in the ERP activity between 600 and 700 ms from S1 onset. This latency corresponded to an interval between 100 and 200 ms following the omission of the imperative stimulus, which was expected at 500 ms on the basis of the global prediction (Fig. 7A; Supplementary Fig. 2; Supplementary Fig. 1). This effect, here defined as the ODP (Mento and Vallesi, 2016) was observed in the SB-L *vs.* the LB-L condition and was expressed over a negative central cluster of electrodes (negative cluster: p = .002 cluster size = −128, cluster statistic = 70; d = −0.76).

The oscillatory results showed that the expectancy violation elicited a synchronization in the delta and theta frequency bands (p = .015; clusters size = 186; cluster statistic = 148). Specifically, the delta increase exhibits a diffuse scalp distribution, covering frontal, central and posterior electrodes while the theta modulation is more localized, closely reflecting the location of the identified ERP effect (see Fig. 7B).

The source analysis revealed a violation-related increase in the electrical activity of the left temporal parietal junction (TPJ), left pre-central

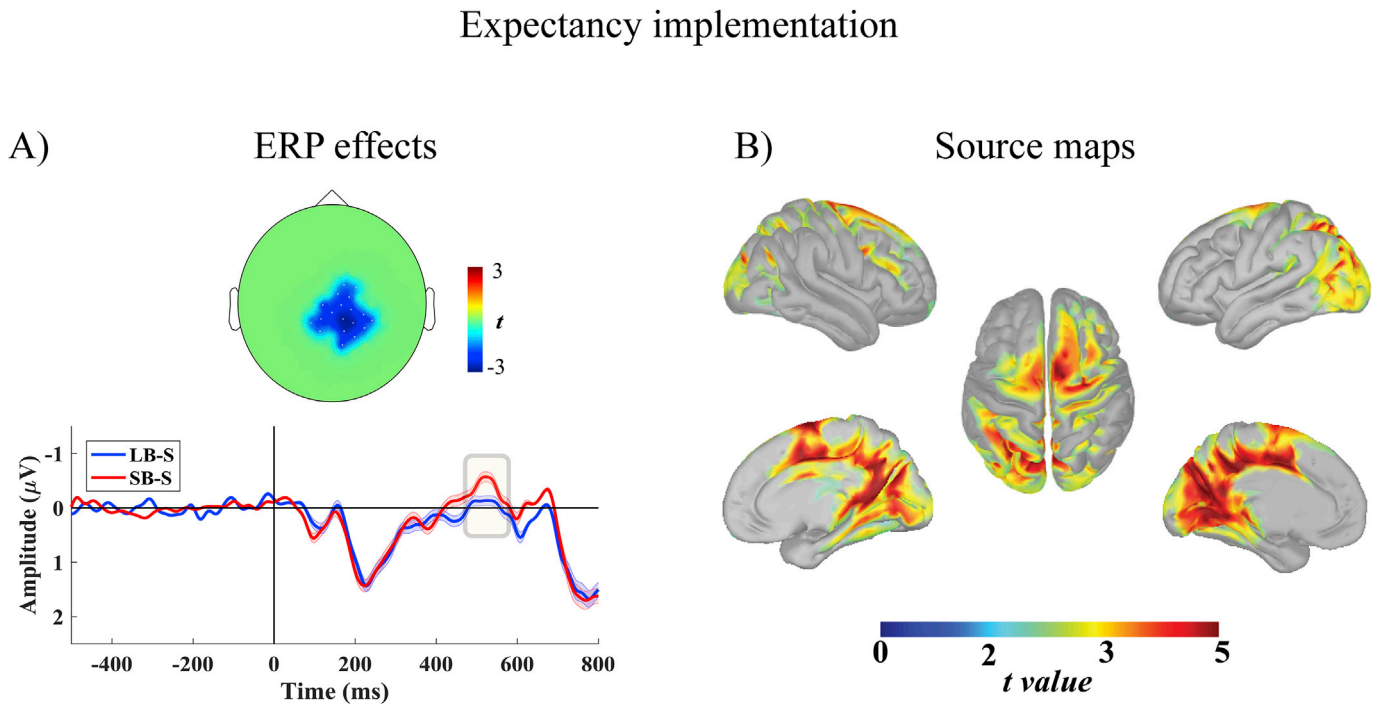

Fig. 5. Global prediction effect on expectancy implementation. **A)** The upper part of the panel represents the statistically significant electrodes ($p < .05$) derived from the cluster based permutation analysis. The negative cluster indicates that CNV mean amplitude is significantly larger in the short-biased than in the long-biased blocks in the last part of the preparation, and this difference is expressed over centro-parietal electrodes. The ERP below the scalp map shows the time series of the negative cluster for the contrasted conditions. The S1 at 0 ms indicates the ERP time locking. The shaded area around the time series represents the standard error. **B)** The panel shows the statistical difference of the source maps in the comparison between SB-S and LB-S mean activity, obtained in the same time window of the CNV modulation. Significant cluster ($p < .01$) are reported on a template cortex smoothed at 30%.

gyrus and bilateral cuneus ($p < .01$) (Fig. 7C).

4. Discussion

In this study we investigated how different sources of implicit temporal prediction shape distinct neurocomputational mechanisms underlying proactive motor control. To this purpose we recorded and analyzed the hdEEG activity from healthy participants undergoing the Dynamic Temporal Prediction task (DTP; Mento et al., 2020; Mento and Granziol, 2020). The DTP is a simple reaction time task purposely designed to elicit both local (i.e., within-trial stimulus hazard rate) and global (i.e., between-block stimulus expectancy bias) temporal prediction. Specifically, the preparatory interval was manipulated within the trial to generate temporal expectancy on the basis of local probabilistic rules. In addition, we introduced a higher-order (global) predictive rule by introducing different types of blocks with different SOA probabilities, leading to a U (same probability per each SOA), an SB (higher probability of short SOA), and an LB (higher probability of long SOA) distribution. The behavioural results revealed that participants were faster at detecting stimuli when these were preceded by long than medium or short preparatory intervals after a warning signal. This finding replicates previous literature, confirming that motor promptness is proactively biased by the local probability of stimulus onset, which accumulates progressively within each single trial, also known as the 'variable foreperiod effect' (Niemi and Naatanen, 1981; Los, 2010; Vallesi, 2010). As expected, this higher anticipatory preparedness occurred at the expenses of reactive inhibitory control, given that participants committed more premature responses in the trials with the longest preparatory foreperiod. In other words, the more participants waited for the stimulus onset, the faster they were to detect it and the higher was the number of premature responses they committed.

In addition to the expected effect of local prediction on behaviour, we showed that the participants' performance was shaped by the global predictive context. This refers to the overall statistical probability to receive the imperative stimulus after a short or long foreperiod, which in the present study was implicitly manipulated between-block by creating block-wise short- and long-biased probabilistic distributions. Importantly, we observed that participants were overall faster at detecting stimuli in the short-biased blocks (in which most of the foreperiods were short) than in the long-biases ones. This pattern suggests that proactive motor control is sensitive to high-level statistical regularities, although people were not explicitly aware of it. As for local prediction, even in this case a higher excitatory threshold during the anticipatory interval turned out into a disruption of reactive inhibitory control. This was revealed by participants committing more premature responses in long trials when these were globally less probable, that is, in the short-biased blocks. In other words, the ability to prepare for a response is guided not only by the local accumulation of preparation but also by the 'history of events' temporal occurrence over time. From a theoretical point of view, our data nicely support the "multiple trace theory of temporal preparation" (Los et al., 2014; Los et al., 2017), which assume that a sort of temporal tag is experienced on each trial and stored to build up a predictive internal model which, in turn, biases attentional and motor resources trial-by-trial. Noteworthy, in the context of the present paradigm it may be important to investigate the presence of transitional effects in the behavioural adaptation in terms of trial-by-trial task speed changes when shifting between two global distributions. However, the use of a random block order presentation did not allow us to further explore any time-on-task learning effect. We are currently planning a follow-up study to address this important issue.

To understand the functional bases of global prediction impact on proactive motor control we analyzed the temporal, oscillatory and spatial neural signatures of different time windows, corresponding to distinct computational stages. These included expectancy implementation, expectancy violation and response implementation. The effect of global prediction on expectancy implementation was reflected in the block-

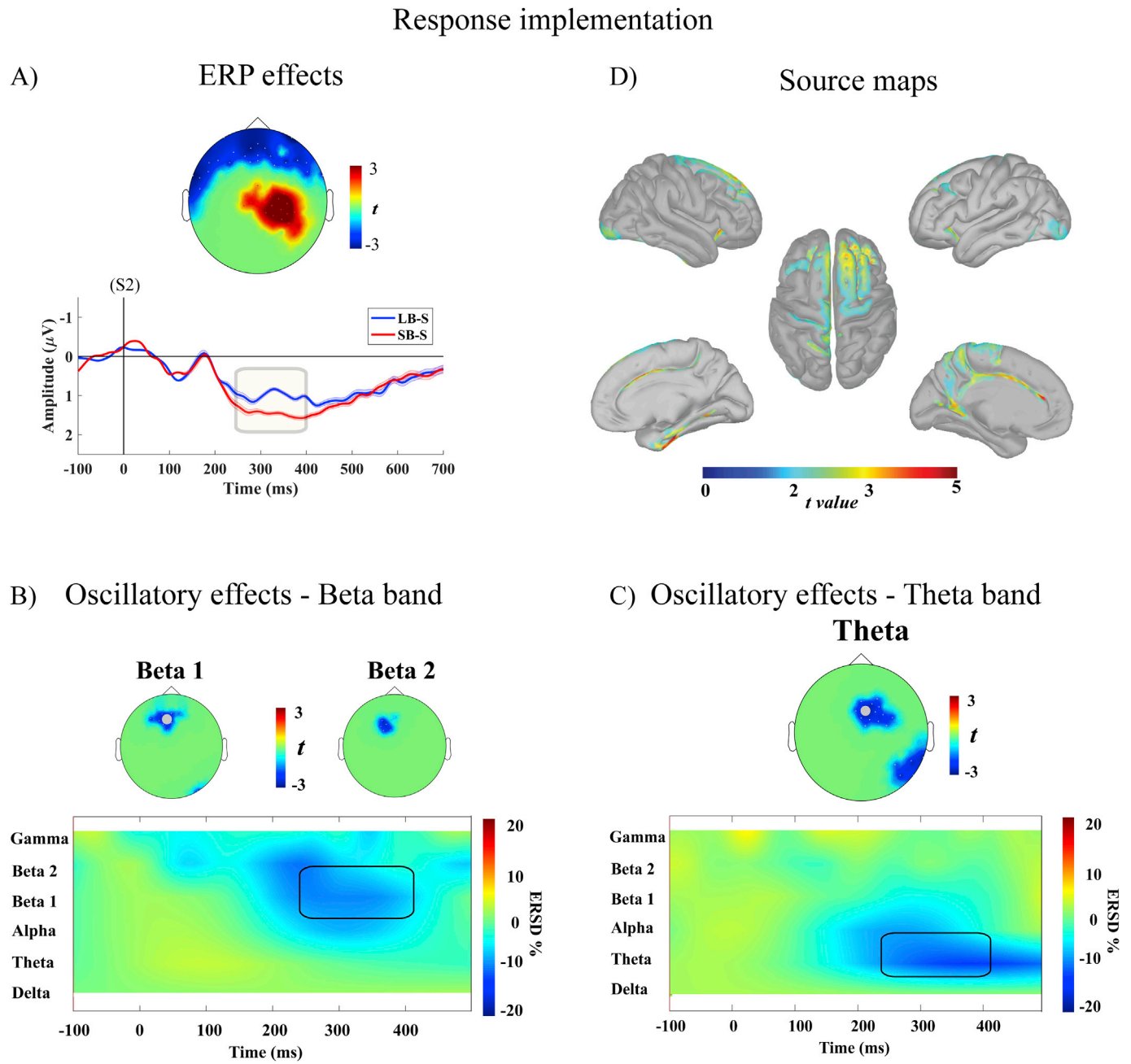

Fig. 6. Global prediction effect on response implementation. **A)** The upper panel displays the statistically significant electrodes ($p < .05$) in reddish or bluish colors, depending on the direction of the *t*-test. At the level of response implementation, the P3 amplitude shows a mean amplitude increase for the expected stimulus (SB–S condition) compared to the unexpected one (LB-S condition). The picture below the scalp map shows the S2-locked time-course of the central positive cluster. The shaded area around the time series represents the standard error. **B)** The raster plot displays the power density statistical difference elicited by response implementation at E22 electrode (FP1 in the 10–20 system; gray dot on the scalp map), separately for the beta1 and beta2 frequency bands. The scalp plots represent the scalp distribution of these effects. **C)** The raster plot displays the power density statistical difference elicited by response implementation at E6 electrode (FCz in the 10–20 system; gray dot on the scalp map), for the theta frequency band. The scalp plot represents the scalp distribution of this effect. **D)** The panel shows the statistical difference of the source maps in the comparison between SB-S and LB-S mean post target activity (250–400 ms). Significant cluster ($p < .01$) are reported on a template cortex smoothed at 30%.

dependent CNV increase around 100 ms before stimulus onset (see Fig. 5A). Remarkably, this marker was modulated as a function of the block-type, being on average larger in the trials with high-probable short intervals (i.e., short-biased blocks) as compared the low-probable ones (i.e., long-biased blocks). This ERP effect nicely aligned with behavioural data, showing that globally-induced faster responses are explained by higher expectancy implementation during the anticipatory interval. The source-level analysis provided further spatial detail to this finding, showing that the higher expectancy implementation is supported by a larger recruitment of a distributed brain cortical network. This circuit mainly entailed the left inferior parietal region (i.e., around the IPS) together with bilateral frontal areas (i.e., the SMA and the motor/pre-motor cortex) (see Fig. 5B). Notably, these findings replicate our previous electrical source-based studies on the effect of temporal expectancy when this is prompted by either explicit cueing task (Mento et al., 2015, 2018; Mento and Vallesi, 2016; Mento, 2017) or implicit manipulations (i.e., sequential effects; Mento, 2017). As well, they replicate findings from independent research groups using other neuroimaging techniques

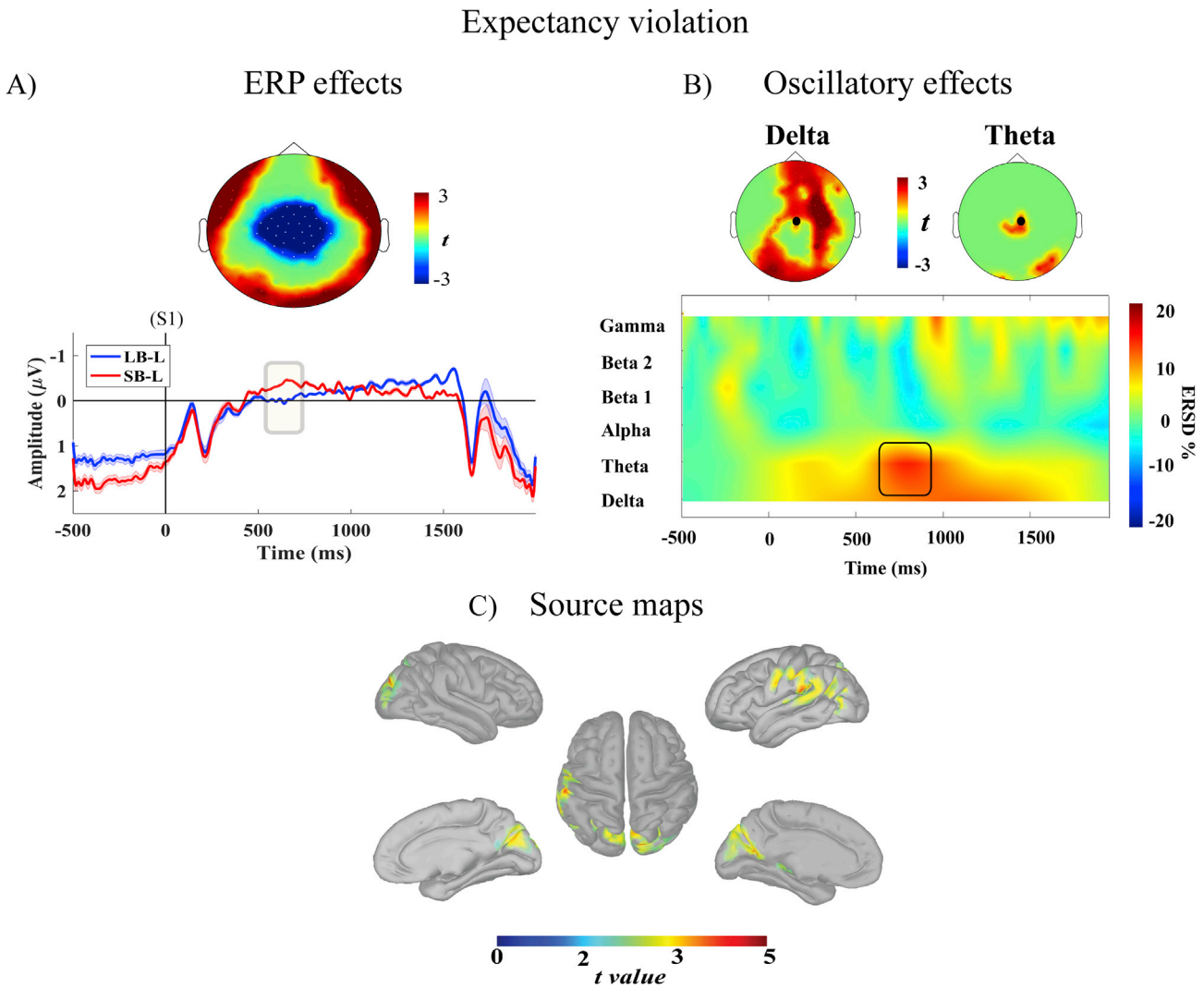

Fig. 7. Global prediction effect on expectancy violation. **A)** The upper part of the panel represents the statistically significant electrodes ($p < .05$) derived from the cluster based permutation analysis. The central negative cluster indicates that the omission evoked potential (ODP) is significantly larger in the SB *vs.* LB blocks between 600 and 700 ms. The ERP below the scalp map shows the S1-locked time course of the central negative cluster. The shaded area around the time series represents the standard error. **B)** The raster plot displays the statistical differential power density for expectancy violation at the E55 electrode (Cz in the 10–20 system; black dot on the scalp map), separately for the delta (right scalp map) and theta (left scalp map) frequency bands. The scalp plots represent the scalp distribution of these effects. **C)** The panel shows the statistical difference of the source maps in the comparison between SB-L and LB-L mean activity in the 600–700 ms time window. Significant cluster ($p < .01$) are reported on a template cortex smoothed at 30%.

(Coull and Nobre, 1998; Coull et al., 2000; Coull, 2004; Coull et al., 2013; Cotti et al., 2011; Nobre, 2001; Davranche et al., 2011; Bolger et al., 2014). This fronto-parietal network has been advocated to functionally mediate the feedforward generation and orientation of attentional and motor resources toward future expected events (see Coull, 2011 for a review). Crucially, for the first time here we report that a similar network is involved when attention and motor preparation are forecasted implicitly on the basis of global predictive information. A theoretical implication of this is that the implementation of expectancy, whether this is generated explicitly or implicitly, is independent from the mechanisms accounting for how this expectation has been generated over time. In other words, the left fronto-parietal network engaged by expectancy implementation may be akin a by-product of the internal temporal predictive model generated on the basis of the environmental experience. In addition to the above mentioned left fronto-parietal network we reported an engagement of the cingulate cortex. Although the role of this structure has been not exhaustively elucidated yet, its involvement may reflect an enhanced need for reactive inhibitory control (Bokura et al., 2001; Braver et al., 2001; Shen et al., 2015). That is, the more participants will engage fronto-parietal activity to speed-up their response proactively, the more they will need to exert reactive inhibitory control to overcome impulsive responses.

The expectancy implementation translates into an increase of neural resources allocated to stimulus detection, as confirmed by a larger P3 following high-than low-predicted targets on the basis of the global predictive context (see Fig. 6A). The neural sources of this effect encompassed several anterior brain areas, including the SMA, the SFG and the ACC. This pattern strongly suggests that part of the network pre-activated during the expectancy implementation was actually involved in the response implementation stage too, reflecting a continuity between the proactive and the reactive motor control.

As an alternative hypothesis, this effect may be the result of an attenuation of the P300 in the LB-S condition, which may be caused by a higher amplitude of motor activity recruited following the relatively unexpected response signal in the LB-S condition. Although interesting, this idea is not entirely supported by the oscillatory patterns we found. Indeed, this showed globally-induced predictive effect, with expected targets triggering an increased beta-band desynchronization in frontal

electrodes contralateral to the response hand (right hand) (see Fig. 6B). The Beta band power decrease has been usually related to the motor preparation and execution, and seems to be generated by the contralateral peri-rolandic regions (Jasper and Penfield, 1949; Tzagarakis et al., 2010; (Pfurtscheller and Berghold, 1989; Sanes and Donoghue, 1993; Murthy and Fetz, 1996; Pfurtscheller and Neuper, 1997; Formaggio et al., 2008). Noteworthy, it has been shown that this neurophysiological mechanism is regulated by the local temporal predictability, either when this is induced voluntarily or implicitly (Mento et al., 2018). Our data further expand upon previous findings by showing a beta desynchronization also for stimuli that are implicitly predicted on the basis of a global predictive context. We also observed an increase in the frontal theta power for the LB-S compared to the SB-S (see Fig. 6C). The frontal midline theta has been interpreted as a general neural hallmark reflecting cognitive control (Cavanagh and Frank, 2014) and rule violation detection (Tzur and Berger, 2009, 2007). We speculate that in the LB condition, where participants were biased to expect stimuli to appear late, the unexpected delivery of the targets in the short interval represented a violation of the global rule, requiring an increase of reactive control demand to adjust behaviour, as suggested by the increase of premature responses. This interpretation may also explain what we observed for the expectancy violation stage, which was investigated comparing the brain activity when the stimulus occurred when expected (LB-L) vs. the rule violation condition (delayed onset; SB-L). Indeed, the participants implicitly generate a global internal predictive model which drives them to be more prepared for the stimulus onset at 500 ms, ergo, a target delay represents a violation of the expectation based on the global prediction. The analyses revealed that the missed target presentation yielded a central negativity peaking between 100 and 200 ms from the expected target onset time (see Fig. 7A). This neural marker has been defined the omission-detection potential (ODP), in line with the ERP we previously reported in response to a violation of local expectancy (Mento and Vallesi, 2016). The expectancy violation was also associated to a synchronization increase in the delta and theta frequency bands (see Fig. 7B). A delta synchronization enhancement has been related to transient inhibitory control of contextual novelty independently from the exogenous or endogenous origin (Prada et al., 2014). A fundamental role of delta has been also purported in the evaluation of internal and external events based on their behavioural saliency (Knyazev, 2012). According to this hypothesis, the augmented delta activity could reflect high behavioral relevance of a change in task context or in the saliency of a stimulus (Huster et al., 2013). Moreover, delta power has been shown to be sensible to the stimulus sequence context information (Harper et al., 2016). On the other side, as above mentioned, the theta frequency band seems to reflect general control process, conveying the information that something needs to be done, although without necessarily carrying the content of what has to be done (Cavangh and Frank, 2014). In our experimental design, the theta synchronization may signal the need for an update of the internal predictive model and a consequential behavioral schema adjustment, such as the inhibition of a prepared response and a subsequent reorienting of the attention to the next time interval. On the other hand, delta synchronization can be related to the active inhibition of the pre-activated motor schema in order to adapt the behaviour to the environmental requests. Accordingly with this hypothesis, we observed an increased activity over of the left precentral gyrus and the TPJ (see Fig. 7C). The engagement of the motor cortex could be explained as the effects of the inhibition of the motor response, on the other side the involvement of TPJ can be linked to the reorienting process. Neuroimaging studies advocated a role for TPJ as a core node of the ventral attentional control network engaged in exogenous (automatic) attentional-reorienting towards unexpected visual target (Corbetta and Shulman, 2002; Chica et al., 2013; Wu et al., 2015; Downar et al., 2002). A complementary interpretation sustains that TPJ engagement can be better understood in terms of 'contextual updating' of an internal model of the environmental setting based on new incoming sensory information (Soltani and Knight, 2000; Polich, 2007; Geng and Vossel, 2013). Our results nicely support both the above interpretations, since the expectancy violation-dependent TPJ activity may underlie an internal model update based on the experience of the new sensory information (i.e. the absence of the expected stimulus onset) and a subsequent attentional re-orienting toward the next, most probable target onset time.

Overall, the present results suggest that cognitive control of motor response can be implicitly driven by both first- (local) or second-order (global) predictive rules. The capability to implicitly extract global statistical patterns of regularities and use them to shift from different proactive control sets is likely linked to the individual cognitive flexibility. Cognitive flexibility has been recognized as a core function of cognitive control (Diamond, 2013; Miyake et al., 2000) and considered a top-down process able to guide the action based on internal goals and external context, requiring therefore volition and attention to down-regulate behaviour (Diamond, 2013; Miller and Cohen, 2001; Norman and Shallice, 1986). However, our results better support a most recent theoretical framework positing that cognitive control can indeed be guided by low level associative learning processes (Braem and Egner, 2018; Crump and Logan, 2010; Sali et al., 2015; Farooqui and Manly, 2015). As we recently proposed in the context of proactive motor control development (Mento and Granziol, 2020), cognitive flexibility can be seen as being rooted in the learning process of 'stimulus-response' associations itself rather than conceived as the by-product of a sort of homuncular, stand-alone superordinate modular structure. An implication of this view is a putative overlapping between the neurocomputational mechanisms underlying voluntary *vs.* implicit proactive motor control. Here we provide empirical support to this hypothesis, showing for the first time that, when high or low motor preparation is implicitly induced by global prediction, the neural signatures in the spatial, temporal and oscillatory domains largely mimic those observed for endogenous control induced by explicit predictive information. This suggests that the two processes are not separated but indeed the two faces of the same coin, providing further support for overcoming the dichotomic contraposition between voluntary-driven cognitive control vs. automatic processes.

5. Conclusions

In this study we provided electrophysiological evidence suggesting that the brain is capable to implicitly adjust proactive motor control based on a simple, low-level associative learning mechanism, i.e., the probabilistic context of an event occurrence. Specifically, the implicit use of global predictive rule translates into an expectancy implementation (CNV increase) and response implementation adjustment (P3 increase), resulting in a better behavioural performance (RT decrease). The expectancy violation induced by the omission of expected target resulted in a general alerting system activation (fronto-central theta synchronization), signaling the need to update the internal predictive model, and to inhibit the pre-activated motor schema (delta synchronization), in order to flexibly adapt motor behaviour. Brain areas engaged during expectancy and response implementation have been identified as part of the fronto-parietal network including inferior parietal lobule, SMA, motor and cingulate cortex. On the other side, left motor cortex and TPJ was mainly involved in the expectancy violation, probably related to the pre-activated motor schema inhibition and internal model update. The limitations in the spatial resolution of the source reconstruction requires caution in the interpretation of the results. Nonetheless, considering the convergence with other source reconstruction and fMRI studies, the present results could be used as a starting point for future confirmatory studies. Our lab is currently doing further research to explore the transitional effects in the behavioural adaptation when shifting between global distributions, resulting in the possibility to model individual learning effects.

CRediT authorship contribution statement

G.M. Duma: Investigation, Methodology, Formal analysis, Visualization, Writing - original draft, Writing - review & editing. **U. Granziol:**

Data curation, Visualization, Writing - original draft. **G. Mento:** Funding acquisition, Investigation, Methodology, Project administration, Writing - original draft, Writing - review & editing.

Acknowledgements

The authors wish to thank Matteo Invidia, Agnese Bernabucci and Antonio Cataneo for helping with data collection. A thank goes also to Prof. Quintana who inspired the present study. The present study was funded by the University of Padova (Supporting TAlent in ReSearch @ University of Padova - STARS Grants 2017 to GM). This work was carried out the scope of the research program "Dipartimenti di Eccellenza" 970 (art.1, commi 314–337 legge 232/2016), which was supported by 971 a grant from MIUR to the Department of General Psychology, 972 University of Padua.

Appendix A. Supplementary data

Supplementary data to this article can be found online at https://doi.org/10.1016/j.neuroimage.2020.117071.

References

Bates, D., Mächler, M., Bolker, B., Walker, S., 2015. Fitting linear mixed-effects models using lme4. J. Stat. Software 67, 1–48. https://doi.org/10.18637/jss.v067.i01.

Baumeister, A.A., Joubert, C.E., 1969. Interactive effects on reaction time of preparatory interval length and preparatory interval frequency. J. Exp. Psychol. 82 (2), 393–395. https://doi.org/10.1037/h0028119.

Bekinschtein, T.A., Dehaene, S., Rohaut, B., Tadel, F., Cohen, L., Naccache, L., 2009. Neural signature of the conscious processing of auditory regularities. Proc. Natl. Acad. Sci. U.S.A. 106 (5), 1672–1677. https://doi.org/10.1073/pnas.0809667106.

Bell, A.J., Sejnowski, T.J., 1995. An information-maximization approach to blind separation and blind deconvolution. Neural Comput. 7 (6), 1129–1159. https://doi.org/10.1162/neco.1995.7.6.1129.

Bokura, H., Yamaguchi, S., Kobayashi, S., 2001. Electrophysiological correlates for response inhibition in a Go/NoGo task. Clin. Neurophysiol. 112 (12), 2224–2232. https://doi.org/10.1016/S1388-2457(01)00691-5.

Bolger, D., Coull, J.T., Schön, D., 2014. Metrical rhythm implicitly orients attention in time as indexed by improved target detection and left inferior parietal activation. J. Cognit. Neurosci. 26 (3), 593–605. https://doi.org/10.1162/jocn_a_00511.

Braem, S., Egner, T., 2018. Getting a grip on cognitive flexibility. Curr. Dir. Psychol. Sci. 27 (6), 470–476. https://doi.org/10.1177/0963721418787475.

Braver, T.S., Barch, D., Gay, J., Molfese, D., Snyder, A., 2001. Anterior cingulate cortex and response conflict: effects of frequency, inhibition and errors. Cerebr. Cortex 11 (9), 825–836.

Breska, A., Deouell, L.Y., 2014. Automatic bias of temporal expectations following temporally regular input independently of high-level temporal expectation. J. Cognit. Neurosci. 26 (7), 1555–1571.

Buiatti, M., Di Giorgio, E., Piazza, M., Polloni, C., Menna, G., Taddei, F., et al., 2019. Cortical route for facelike pattern processing in human newborns. Proc. Natl. Acad. Sci. U.S.A. 116 (10), 4625–4630. https://doi.org/10.1073/pnas.1812419116.

Capizzi, M., Correa, Á., Sanabria, D., 2013. Temporal orienting of attention is interfered by concurrent working memory updating. Neuropsychologia 51 (2), 326–339. https://doi.org/10.1016/j.neuropsychologia.2012.10.005.

Capizzi, M., Ambrosini, E., Arbula, S., Mazzonetto, I., Vallesi, A., 2016. Electrophysiological evidence for domain-general processes in task-switching. Front. Hum. Neurosci. 10 (March), 1–14. https://doi.org/10.3389/fnhum.2016.00124.

Cavanagh, J.F., Frank, M.J., 2014. Frontal theta as a mechanism for cognitive control. Trends Cognit. Sci. 18 (8), 414–421. https://doi.org/10.1016/j.tics.2014.04.012.

Chennu, S., Noreika, V., Gueorguiev, D., Blenkmann, A., Kochen, S., Ibanez, A., et al., 2013. Expectation and attention in hierarchical auditory prediction. J. Neurosci. 33 (27), 11194–11205. https://doi.org/10.1523/JNEUROSCI.0114-13.2013.

Chica, A.B., Bartolomeo, P., Lupiáñez, J., 2013. Two cognitive and neural systems for endogenous and exogenous spatial attention. Behav. Brain Res. 237 (1), 107–123. https://doi.org/10.1016/j.bbr.2012.09.027.

Clark, A., 2013. Whatever next? Predictive brains, situated agents, and the future of cognitive science. Behav. Brain Sci. 36 (3), 181–204. https://doi.org/10.1017/S0140525X12000477.

Corbetta, M., Shulman, G.L., 2002. Control of goal-directed and stimulus-driven attention in the brain. Nat. Rev. Neurosci. 3 (3), 201–215. https://doi.org/10.1038/nrn755.

Correa, Á., Nobre, A.C., 2008. Neural modulation by regularity and passage of time. J. Neurophysiol. 100 (3), 1649–1655. https://doi.org/10.1152/jn.90656.2008.

Correa, Á., Lupiáñez, J., Tudela, P., 2006. The attentional mechanism of temporal orienting: determinants and attributes. Exp. Brain Res. 169 (1), 58–68. https://doi.org/10.1007/s00221-005-0131-x.

Cotti, J., Rohenkohl, G., Stokes, M., Nobre, A.C., Coull, J.T., 2011. Functionally dissociating temporal and motor components of response preparation in left intraparietal sulcus. Neuroimage 54 (2), 1221–1230. https://doi.org/10.1016/j.neuroimage.2010.09.038.

Coull, J.T., 2004. fMRI studies of temporal attention: allocating attention within, or towards, time. Cognit. Brain Res. 21 (2), 216–226. https://doi.org/10.1016/j.cogbrainres.2004.02.011.

Coull, J.T., Nobre, A.C., 1998. Where and when to pay attention: the neural systems for directing attention to spatial locations and to time intervals as revealed by both PET and fMRI. J. Neurosci. 18 (18), 7426–7435.

Coull, J.T., Nobre, A.C., 2008. Dissociating explicit timing from temporal expectations with fMRI. Curr. Opin. Neurobiol. 18, 137–144.

Coull, J.T., Frith, C.D., Büchel, C., Nobre, A.C., 2000. Orienting attention in time: behavioural and neuroanatomical distinction between exogenous and endogenous shifts. Neuropsychologia 38 (6), 808–819. https://doi.org/10.1016/S0028-3932(99)00132-3.

Coull, J.T., Davranche, K., Nazarian, B., Vidal, F., 2013. Functional anatomy of timing differs for production versus prediction of time intervals. Neuropsychologia 51 (2), 309–319. https://doi.org/10.1016/j.neuropsychologia.2012.08.017.

Crump, M.J.C., Logan, G.D., 2010. Hierarchical control and skilled typing: evidence for word-level control over the execution of individual keystrokes. J. Exp. Psychol. Learn. Mem. Cognit. 36 (6), 1369–1380. https://doi.org/10.1037/a0020696.

Cui, X., Stetson, C., Montague, P.R., Eagleman, D.M., 2009. Ready go: amplitude of the fMRI signal encodes expectation of cue arrival time. PLoS Biol. 7 (8) https://doi.org/10.1371/journal.pbio.1000167.

Davranche, K., Nazarian, B., Vidal, F., Coull, J., 2011. Orienting attention in time activates left intraparietal sulcus for both perceptual and motor task goals. J. Cognit. Neurosci. 23 (11), 3318–3330. https://doi.org/10.1162/jocn_a_00030.

Delorme, A., Makeig, S., 2004. EEGLAB: an open source toolbox for analysis of single-trial EEG dynamics including independent component analysis. J. Neurosci. Methods 134 (1), 9–21. https://doi.org/10.1016/j.jneumeth.2003.10.009.

Doherty, J.R., Rao, A., Mesulam, M.M., Nobre, A.C., 2005. Synergistic effect of combined temporal and spatial expectations on visual attention. J. Neurosci. 25 (36), 8259–8266. https://doi.org/10.1523/JNEUROSCI.1821-05.2005.

Downar, J., Crawley, A.P., Mikulis, D.J., Davis, K.D., 2002. A cortical network sensitive to stimulus salience in a neutral behavioral context across multiple sensory modalities. J. Neurophysiol. 87 (1), 615–620. https://doi.org/10.1152/jn.00636.2001.

Duma, G.M., Mento, G., Cutini, S., Sessa, P., Baillet, S., Brigadoi, S., Dell'Acqua, R., 2019. Functional dissociation of anterior cingulate cortex and intraparietal sulcus in visual working memory. Cortex 121, 277–291. https://doi.org/10.1016/j.cortex.2019.09.009.

Evans, A.C., Janke, A.L., Collins, D.L., Baillet, S., 2012. Brain templates and atlases. Neuroimage 62 (2), 911–922. https://doi.org/10.1016/j.neuroimage.2012.01.024.

Farooqui, A.A., Manly, T., 2015. Anticipatory control through associative learning of subliminal relations: invisible may Be better than visible. Psychol. Sci. 26 (3), 325–334. https://doi.org/10.1177/0956797614564191.

Faul, F., Erdfelder, E., Lang, A.-G., Buchner, A., 2007. G*Power 3: a flexible statistical power analysis program for the social, behavioral, and biomedical sciences. Behav. Res. Methods 39, 175–191.

Ferree, T.C., 2006. Spherical splines and average referencing in scalp electroencephalography. Brain Topogr. 19 (1–2), 43–52. https://doi.org/10.1007/s10548-006-0011-0.

Formaggio, E., Storti, S.F., Avesani, M., Cerini, R., Milanese, F., Gasparini, A., et al., 2008. EEG and fMRI coregistration to investigate the cortical oscillatory activities during finger movement. Brain Topogr. 21 (2), 100–111. https://doi.org/10.1007/s10548-008-0058-1.

Friston, K., 2010. The free-energy principle: a unified brain theory? Nat. Rev. Neurosci. 11 (2), 127–138. https://doi.org/10.1038/nrn2787.

Geng, J.J., Vossel, S., 2013. Re-evaluating the role of TPJ in attentional control: contextual updating? Neurosci. Biobehav. Rev. 37 (10), 2608–2620. https://doi.org/10.1016/j.neubiorev.2013.08.010.

Gramfort, A., Papadopoulo, T., Olivi, E., Clerc, M., 2011. Forward Field Computation with OpenMEEG, vol. 2011. Computational Intelligence and Neuroscience. https://doi.org/10.1155/2011/923703.

Groppe, D.M., Urbach, T.P., Kutas, M., 2011. Mass univariate analysis of event-related brain potentials/fields I: a critical tutorial review. Psychophysiology 48 (12), 1711–1725. https://doi.org/10.1111/j.1469-8986.2011.01273.x.

Harper, J., Malone, S.M., Bachman, M.D., Bernat, E.M., 2016. Stimulus sequence context differentially modulates inhibition-related theta and delta band activity in a go/no-go task. Psychophysiology 53 (5), 712–722. https://doi.org/10.1111/psyp.12604.

Huster, R.J., Enriquez-Geppert, S., Lavallee, C.F., Falkenstein, M., Herrmann, C.S., 2013. Electroencephalography of response inhibition tasks: functional networks and cognitive contributions. Int. J. Psychophysiol. 87 (3), 217–233. https://doi.org/10.1016/j.ijpsycho.2012.08.001.

Jasper, H., Penfield, W., 1949. Electrocorticograms in man: effect of voluntary movement upon the electrical activity of the precentral gyrus. Archiv Für Psychiatrie Und Nervenkrankheiten 183 (1–2), 163–174. https://doi.org/10.1007/BF01062488.

Johnson, K.A., Burrowes, E., Coull, J.T., 2015. Children can implicitly, but not voluntarily, direct attention in time. PloS One 10 (4), 1–15. https://doi.org/10.1371/journal.pone.0123625.

Karlin, L., 1958. Reaction time as a function of foreperiod duration and variability. J. Exp. Psychol. 58 (2), 185–191.

Knyazev, G.G., 2012. EEG delta oscillations as a correlate of basic homeostatic and motivational processes. Neurosci. Biobehav. Rev. 36 (1), 677–695. https://doi.org/10.1016/j.neubiorev.2011.10.002.

Kotowski, K., Stapor, K., Leski, J., 2019. Improved robust weighted averaging for event-related potentials in EEG. BioCyber. Biomed. Eng. 39 (4), 1036–1046. https://doi.org/10.1016/j.bbe.2019.09.002.

Kybic, J., Clerc, M., Faugeras, O., Keriven, R., Papadopoulo, T., 2005. Fast multipole acceleration of the MEG/EEG boundary element method. Phys. Med. Biol. 50 (19), 4695–4710. https://doi.org/10.1088/0031-9155/50/19/018.
Łęski, J.M., 2002. Robust weighted averaging. IEEE (Inst. Electr. Electron. Eng.) Trans. Biomed. Eng. 49 (8), 796–804. https://doi.org/10.1109/TBME.2002.800757.
Los, S.A., 2010. Foreperiod and sequential effects: theory and data. In: Coull, J., Nobre, A.C. (Eds.), In *Attention And Time*. Oxford University Press, Oxford,UK, pp. 289–302.
Los, S.A., Heslenfeld, D.J., 2005. Intentional and unintentional contributions to nonspecific preparation: electrophysiological evidence. J. Exp. Psychol. Gen. 134 (1), 52–72. https://doi.org/10.1037/0096-3445.134.1.52.
Los, S.A., Kruijne, W., Meeter, M., 2014. Outlines of a multiple trace theory of temporal preparation. Front. Psychol. 5 (SEP), 1–13. https://doi.org/10.3389/fpsyg.2014.01058.
Los, S.A., Kruijne, W., Meeter, M., 2017. Hazard versus history: temporal preparation is driven by past experience. J. Exp. Psychol. Hum. Percept. Perform. 43 (1), 78–88. https://doi.org/10.1037/xhp0000279.
Macar, F., Vidal, F., 2004. Event-related potentials as indices of time processing: a review. J. Psychophysiol. 18 (2–3), 89–104. https://doi.org/10.1027/0269-8803.18.23.89.
Marti, S., Thibault, L., Dehaene, S., 2014. How does the extraction of local and global auditory regularities vary with context? PloS One 9 (9). https://doi.org/10.1371/journal.pone.0107227.
Mento, G., 2013. The passive CNV: carving out the contribution of task-related processes to expectancy. Front. Hum. Neurosci. 7 (December), 1–5. https://doi.org/10.3389/fnhum.2013.00827.
Mento, G., 2017. The role of the P3 and CNV components in voluntary and automatic temporal orienting: a high spatial-resolution ERP study. Neuropsychologia 107 (September), 31–40. https://doi.org/10.1016/j.neuropsychologia.2017.10.037.
Mento, G., Granziol, U., 2020. The developing predictive brain: how implicit temporal expectancy induced by local and global prediction shapes action preparation across development. Dev. Sci. 1–13. https://doi.org/10.1111/desc.12954. April 2019.
Mento, G., Tarantino, V., 2015. Developmental trajectories of internally and externally driven temporal prediction. PloS One 10 (8), 1–18. https://doi.org/10.1371/journal.pone.0135098.
Mento, G., Valenza, E., 2016. Spatiotemporal neurodynamics of automatic temporal expectancy in 9-month old infants. Sci. Rep. 6 (January), 1–10. https://doi.org/10.1038/srep36525.
Mento, G., Vallesi, A., 2016. Spatiotemporally dissociable neural signatures for generating and updating expectation over time in children: a High Density-ERP study. Deve. Cognitive Neurosci. 19, 98–106. https://doi.org/10.1016/j.dcn.2016.02.008.
Mento, G., Tarantino, V., Sarlo, M., Bisiacchi, P.S., 2013. Automatic temporal expectancy: a high-density event-related potential study. PloS One 8 (5). https://doi.org/10.1371/journal.pone.0062896.
Mento, G., Tarantino, V., Vallesi, A., Bisiacchi, P.S., 2015. Spatiotemporal neurodynamics underlying internally and externally driven temporal prediction: a high spatial resolution ERP study. J. Cognit. Neurosci. 27 (3), 425–439. https://doi.org/10.1162/jocn_a_00715.
Mento, G., Astle, D.E., Scerif, G., 2018. Cross-frequency phase–amplitude coupling as a mechanism for temporal orienting of attention in childhood. J. Cognit. Neurosci. 30 (4), 594–602. https://doi.org/10.1162/jocn_a_01223.
Mento, G., Scerif, G., Granziol, U., Franzoi, M., Lanfranchi, S., 2020. The effect of probabilistic context on implicit temporal expectations in down syndrome. Front. Psychol. 11 (March), 1–10. https://doi.org/10.3389/fpsyg.2020.00369.
Miller, E.K., Cohen, J.D., 2001. An integrative theory of prefrontal cortex function. Annu. Rev. Neurosci. 24 (1), 167–202. https://doi.org/10.1146/annurev.neuro.24.1.167.
Miniussi, C., Wilding, E.L., Coull, J.T., Nobre, A.C., 1999. Orienting attention in time. Modul. Brain Potent. 122 (8), 1507–1518. https://doi.org/10.1093/brain/122.8.1507.
Miyake, A., Friedman, N.P., Emerson, M.J., Witzki, A.H., Howerter, A., Wager, T.D., 2000. The unity and diversity of executive functions and their contributions to complex "frontal lobe" tasks: a latent variable analysis. Cognit. Psychol. 41 (1), 49–100. https://doi.org/10.1006/cogp.1999.0734.
Murthy, V.N., Fetz, E.E., 1996. Synchronization of neurons during local field potential oscillations in sensorimotor cortex of awake monkeys. J. Neurophysiol. 76 (6), 3968–3982. https://doi.org/10.1152/jn.1996.76.6.3968.
Niemi, P., Näätänen, R., 1981. Foreperiod and simple reaction time. Psychol. Bull. 89 (1), 133–162. https://doi.org/10.1037/0033-2909.89.1.133.
Nobre, A.C., Van Ede, F., 2018. Anticipated moments: temporal structure in attention. Nat. Rev. Neurosci. 19 (1), 34–48. https://doi.org/10.1038/nrn.2017.141.
Nobre, A., Correa, A., Coull, J., 2007. The hazards of time. Curr. Opin. Neurobiol. 17 (4), 465–470. https://doi.org/10.1016/j.conb.2007.07.006.
Oostenveld, R., Fries, P., Maris, E., Schoffelen, J.M., 2011. FieldTrip: open source software for advanced analysis of MEG, EEG, and invasive electrophysiological data. Comput. Intell. Neurosci. 2011 https://doi.org/10.1155/2011/156869.
Perrin, F., Pernier, J., Bertrand, O., Echallier, J.F., 1989. Perrin_1989_m4.pdf, pp. 184–187.
Pfurtscheller, G., Berghold, A., 1989. Patterns of cortical activation during planning of voluntary movement. Electroencephalogr. Clin. Neurophysiol. 72 (3), 250–258. https://doi.org/10.1016/0013-4694(89)90250-2.
Pfurtscheller, G., Lopes, F.H., 1999. Event-related EEG/MEG synchronization and. Clin. Neurophysiol. 110, 10576479.
Pfurtscheller, G., Neuper, C., 1997. Motor imagery activates primary sensorimotor area in humans. Neurosci. Lett. 239 (2–3), 65–68. https://doi.org/10.1016/S0304-3940(97)00889-6.
Polich, J., 2007. Updating P300: an integrative theory of P3a and P3b. Clin. Neurophysiol. 118 (10), 2128–2148. https://doi.org/10.1016/j.clinph.2007.04.019.
Praamstra, P., Kourtis, D., Kwok, H.F., Oostenveld, R., 2006. Neurophysiology of implicit timing in serial choice reaction-time performance. J. Neurosci. 26 (20), 5448–5455.
Prada, L., Barceló, F., Herrmann, C.S., Escera, C., 2014. EEG delta oscillations index inhibitory control of contextual novelty to both irrelevant distracters and relevant task-switch cues. Psychophysiology 51 (7), 658–672. https://doi.org/10.1111/psyp.12210.
Sali, A.W., Anderson, B.A., Yantis, S., 2015. Learned states of preparatory attentional control. J. Exp. Psychol. Learn. Mem. Cognit. 41 (6), 1790–1805. https://doi.org/10.1037/xlm0000146.
Sanes, J.N., Donoghue, J.P., 1993. Oscillations in local field potentials of the primate motor cortex during voluntary movement. Proc. Natl. Acad. Sci. U.S.A. 90 (10), 4470–4474. https://doi.org/10.1073/pnas.90.10.4470.
Shen, C., Ardid, S., Kaping, D., Westendorff, S., Everling, S., Womelsdorf, T., 2015. Anterior cingulate cortex cells identify process-specific errors of attentional control prior to transient prefrontal-cingulate inhibition. Cerebr. Cortex 25 (8), 2213–2228. https://doi.org/10.1093/cercor/bhu028.
Soltani, M., Knight, R.T., 2000. Neural origins of the P300. Crit. Rev. Neurobiol. 14 (3–4), 199–224. https://doi.org/10.1615/critrevneurobiol.v14.i3-4.20.
Strauss, M., Sitt, J.D., King, J.-R., Elbaz, M., Azizi, L., Buiatti, M., et al., 2015. Disruption of hierarchical predictive coding during sleep. Proc. Natl. Acad. Sci. Unit. States Am. 112 (11), E1353–E1362. https://doi.org/10.1073/pnas.1501026112.
Tadel, F., Baillet, S., Mosher, J.C., Pantazis, D., Leahy, R.M., 2011. Brainstorm: a user-friendly application for MEG/EEG analysis. Comput. Intell. Neurosci. 2011 https://doi.org/10.1155/2011/879716.
Trillenberg, P., Verleger, R., Wascher, E., Wauschkuhn, B., Wessel, K., 2000. CNV and temporal uncertainty with "ageing" and "non-ageing" S1-S2 intervals. Clin. Neurophysiol. 111 (7), 1216–1226. https://doi.org/10.1016/S1388-2457(00)00274-1.
Tzagarakis, C., Ince, N.F., Leuthold, A.C., Pellizzer, G., 2010. Beta-band activity during motor planning reflects response uncertainty. J. Neurosci. 30 (34), 11270–11277. https://doi.org/10.1523/JNEUROSCI.6026-09.2010.
Tzur, G., Berger, A., 2007. When things look wrong: theta activity in rule violation. Neuropsychologia 45 (13), 3122–3126. https://doi.org/10.1016/j.neuropsychologia.2007.05.004.
Tzur, G., Berger, A., 2009. Fast and slow brain rhythms in rule/expectation violation tasks: focusing on evaluation processes by excluding motor action. Behav. Brain Res. 198 (2), 420–428. https://doi.org/10.1016/j.bbr.2008.11.041.
Vallesi, A., 2010. Neuro-anatomical substrates of foreperiod effects. In: Coull, J.T., Nobre, A.C. (Eds.), In *Attention And Time*. Oxford University Press, Oxford, UK, pp. 303–316.
Vallesi, A., Shallice, T., 2007. Developmental dissociations of preparation over time: deconstructing the variable foreperiod phenomena. J. Exp. Psychol. Hum. Percept. Perform. 33 (6), 1377–1388. https://doi.org/10.1037/0096-1523.33.6.1377.
Visalli, A., Capizzi, M., Ambrosini, E., Mazzonetto, I., Vallesi, A., 2019. Bayesian modeling of temporal expectations in the human brain. Neuroimage 202 (July), 116097. https://doi.org/10.1016/j.neuroimage.2019.116097.
Wacongne, C., Changeux, J.P., Dehaene, S., 2012. A neuronal model of predictive coding accounting for the mismatch negativity. J. Neurosci. 32 (11), 3665–3678. https://doi.org/10.1523/JNEUROSCI.5003-11.2012.
Walter, W.G., Cooper, R., Aldridge, V.J., McCallum, W.C., Winter, A.L., 1964. Contingent negative variation: an electric sign of sensori-motor association and expectancy in the human brain. Nature 203 (4943), 380–384. https://doi.org/10.1038/203380a0.
Woodrow, H., 1914. The measurement of attention. Psychol. Monogr. 17 (5), 1–158.
Wu, Q., Chang, C.F., Xi, S., Huang, I.W., Liu, Z., Juan, C.H., et al., 2015. A critical role of temporoparietal junction in the integration of top-down and bottom-up attentional control. Hum. Brain Mapp. 36 (11), 4317–4333. https://doi.org/10.1002/hbm.22919.
Zandbelt, B.B., Bloemendaal, M., Neggers, S.F.W., Kahn, R.S., Vink, M., 2013. Expectations and violations: delineating the neural network of proactive inhibitory control. Hum. Brain Mapp. 34 (9), 2015–2024. https://doi.org/10.1002/hbm.22047.
Zanto, T.P., Pan, P., Liu, H., Bollinger, J., Nobre, A.C., Gazzaley, A., 2011. Age-related changes in orienting attention in time. J. Neurosci. 31 (35), 12461–12470. https://doi.org/10.1523/jneurosci.1149-11.2011.